Low speed flutter and post-critical behaviour of flat plate and NACA0018 section models in a wind tunnel

Xavier Amandolese

LOW SPEED FLUTTER AND POST-CRITICAL BEHAVIOUR OF FLAT PLATE AND NACA0018 SECTION MODELS IN A WIND TUNNEL

X. Amandolese[+1,2]
[+1] LadHyX, Ecole Polytechnique-CNRS, Palaiseau, France
[+2] CNAM (Conservatoire National des Arts et Métiers), Paris, France

This paper explores the post-critical behaviour of two-degree-of-freedom flat plate and NACA0018 section model undergoing coupled-mode flutter in a wind tunnel. Tests are performed at moderate Reynolds number $Re \sim 1 - 8 \times 10^4$ using an aeroelastic set-up that enables high amplitude pitch-plunge motion without nonlinear structural limitations. For both models, two aeroelastic configurations have been studied: for a centre of rotation at the first quarter chord and for a centre of rotation at the mid-chord. Each configuration exhibits self-limited oscillations du to nonlinear aerodynamics saturation beyond the critical velocity. However, limit cycle oscillations (LCOs) evolution versus the reduced velocity highlight strong different behaviours between the flat plate and the NACA0018 model, along with a significant impact of the position of the elastic center. For the flat plate model two LCOs branches have been found in the post-critical regime. The first one is reached increasing the velocity beyond the coupled-mode flutter critical velocity and the second one occurs when the LCOs amplitude in pitch enter the stall region. This second LCO branch is then associated to a symmetric stall flutter regime. For the flat plate model the switch to symmetric stall flutter has only been observed for the configuration with the elastic axis at the mid-chord. For the NACA0018 model two LCOs branches have also been observed but the dynamical responses are also significantly impacted by a pure pitch instability that can be attributed to the motion-induced dynamics of a laminar separation bubble at moderate Reynolds number.

Keyword: low speed flutter, limit cycle oscillation, nonlinear aeroelasticity, stall flutter, wind tunnel

1. INTRODUCTION

Observed since the early days of flight the coupled-mode flutter of airplane wing is a dynamic instability for which self-sustained oscillations of great violence occurs above a critical speed. Often called "classical" flutter this instability involves at least two modes of the system and, unlike the stall flutter, its onset does not rely on any flow separation. It can hence be observed on wing with no angle of attack if not properly designed. Theory of flutter based upon linear unsteady aerodynamic formulations has been successfully developed to predict the critical conditions for the generic case of a two degrees of freedom "pitch-plunge" oscillating wing (Theodorsen[1)]; Sears[2)]). Since those early works the physical explanation of bending-torsion flutter has also been highlighted (see for example Fung[3)], Bisplinghoff and Ashley[4)] or Dowell[5)]). It is now well understood that the classical flutter relies on fluid-elastic coupling between the structural modes. Indeed combined plunging and pitching motions can produce, above a critical flow velocity, interactions and phase shifts in a way that energy is transferred from the flow to the structure.

Unlike classical flutter, stall flutter is a dynamic instability that does not depend on coupling (Naudascher and Rockwell[6)]). This phenomenon is of particular importance for wing or blade operating at high angle of attack as for helicopter aerodynamics[7)] and wind turbine blades[8)]. In such cases torsion is the mode of vibration most commonly involved. The mechanism for energy transfer then relies on a dynamic stall process for which the flow separates partially or completely during each cycle of oscillation[6)]. Due to the nonlinear nature of the aerodynamic load involved, stall flutter is limited in amplitude (McCroskey[9)], Li and

[+1]xavier.amandolese@ladhyx.polytechnique.fr

Dimitriadis[10]). Many studies have been devoted to the dynamic stall process experienced by a wing oscillating around the static stall angle of attack (McCroskey and Philippe[11]; Carr et al[12]).

Regarding coupled-mode or stall flutter of airfoils numerous investigations on the post-critical behaviour can be found. Most of this studies focus on the impact of nonlinearities encountered in aeronautics (see Dowell et al[13] and Lee et al[14] for a review), such as the impact of concentrated structural nonlinearities[15], control surface freeplay[16], shock wave motion in transonic flow[17] or stall flutter of airfoil[18,19,20]. Recent experimental studies performed by Dimitriadis & Li[21] and Razak et al[22] using a pitch-plunge section model setup are also to be mentioned. In the former study experiments conducted on a NACA0012 section model focussed on the bifurcation behaviour to stall flutter after large perturbation are imposed to the system. In the later study the authors mainly focused on the effect of the mean static angle of a NACA0018 section model to the dynamical response of the system. Price and Fragiskatos[23] also performed a numerical aeroealastic study on a two-degree-of-freedom pitch-plunge airfoil using a dynamic stall model for the prediction of the high amplitude nonlinear unsteady aerodynamics. They identified limit cycle oscillations (LCO) beyond the critical velocity and a gradual increase of LCO amplitude with the velocity, which was recently confirmed experimentally by Amandolese et al[24].

In the new and challenging field of energy harvesting through fluid-structure instabilities, the coupled-mode flutter mechanism has been recently scrutinized[25,26]. A greater focus on post-critical behaviour is however necessary in order to improve the characterization, physical understanding and modeling of the large amplitude self-sustained vibrations resulting from these instabilities. The aim of this paper is to provide experimental results in that context.

The paper is organized as follows: the experimental set-up along with the relevant non-dimensional parameters of the four tested configurations are presented in section 2. Post-critical flutter results are then reported and discussed in Section 3, highlighting LCOs amplitudes and frequencies evolutions with the reduced velocity.

2. EXPERIMENTAL SET-UP

The experiments were performed on two section models: a rigid flat rectangular steel plate of span E=0.225m, chord length c =0.035m and thickness t_c=0.0015m, corresponding to a thickness-to-chord ratio of 4.3% and a NACA0018 section model of span E=0.225m and chord length c =0.04m, made of aluminum. For the NACA0018 model, sand grains were glued near the leading edge in order to trigger the boundary layer laminar-turbulent transition.

Each model was flexibly mounted in plunge and pitch in a small Eiffel wind tunnel (Fig. 1), with a closed rectangular test-section of 0.26 m width and 0.24 m height. A particular attention was paid to the design of a set-up that can allow high amplitude linear response in pitch and plunge. Small chord dimension have been chosen for both models in order to limit blockage effects for high amplitude oscillations. End plates were also mounted at each extremity in order to limit end effects. The set-up is shown in Fig. 1.

The vertical stiffness of the system was set by two long steel laminated springs and two sets of additional linear springs. The axis of rotation was linked to the laminated springs by two bearings mounted at both end and the rotational stiffness was set by two spiral torsion springs. For each section model two position of the centre of rotation have been tested: at the first quarter chord and at the mid-chord. Results will then be presented for four aeroelastic configurations named: “FP14”, “FP12” for the flat-plate with axis of rotation at the first quarter chord and mid-chord respectively and “N14”, “N12” for the NACA18 model with axis of rotation at the first quarter and mid chord respectively.

Tests were performed for a mean velocity in the test-section varying from 4 to 30m/s, with a turbulence level less than 0.4% over this velocity range. In the present study the mean angle of attack of the model is set to zero.

The two degrees of freedom $h(t)$ and $\alpha(t)$ (see Fig. 1) were measured using two laser displacement sensors connected to a 24 bits resolution acquisition system. The first one directly measured the vertical plunging motion at the elastic axis, while the second one measured the combined movement in plunge and

pitch. Recovery of the physical quantities $h(t)$ and $\alpha(t)$ was performed by numerical post-processing with an accuracy less than 2%. The sampling frequency was chosen as 1024Hz and spectral analysis was performed on time block over 8 seconds which gives a frequency resolution lower than 0.125 Hz.

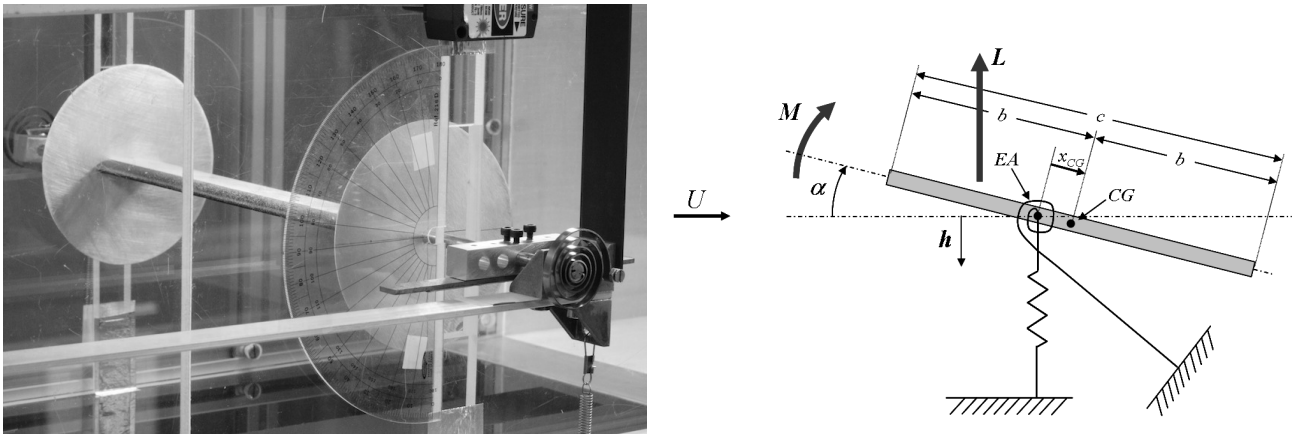

Figure 1: Side view of the setup with the NACA0018 section model (left); definitions and notations of the aeroelastic setup (right).

(2.1) Stuctural parameters

Under zero wind condition, the linearized equations of motion can be expressed as in Eq. 1 :

$$\begin{aligned} m\ddot{h} + D_h\dot{h} + K_h h + S_\alpha\ddot{\alpha} = 0, \\ I_\alpha\ddot{\alpha} + D_\alpha\dot{\alpha} + K_\alpha\alpha + S_\alpha\ddot{h} = 0, \end{aligned} \tag{1}$$

where the parameters $m, I_\alpha, D_h, D_\alpha, K_h, K_\alpha$, are the system's mass, moment of inertia about the elastic axis, structural damping and stiffness in plunge and pitch, respectively. $S_\alpha = mx_{CG}$ is the static moment about the elastic axis, positive if the distance x_{CG} from the elastic axis to the centre of gravity is positive. A static weight calibration technique was used to measure both the stiffness in plunge and pitch. Free decay tests were performed for each degree of freedom taken independently (the other one being locked) to identify the natural frequencies, $\omega_h = \sqrt{K_h/m}$ and $\omega_\alpha = \sqrt{K_\alpha/I_\alpha}$ by spectral analysis, and the damping ratios, $\eta_h = D_h/2\sqrt{K_h m}$ and $\eta_\alpha = D_\alpha/2\sqrt{K_\alpha I_\alpha}$ using a standard decrement technique. The total mass m and inertia I_α of the system were then calculated using the measured stiffness and natural frequencies.
The static unbalance of the section model about the elastic axis S_α was identified using the following expression (see Bisplinghoff and Ashley[4]):

$$S_\alpha = \sqrt{mI_\alpha\left(1 - \frac{\omega_h^2+\omega_\alpha^2}{\omega_1^2+\omega_2^2}\right)}, \tag{2}$$

where ω_1 and ω_2 are the natural frequencies of the coupled system.

A particular attention was devoted to design a setup that allows a structural linear behaviour in stiffness and damping. Static calibration that has been performed showed that the bending stiffness behaves linearly in the range -0.6 ≤ *h/b* ≤ 0.6 and that the stiffness in rotation is linear up to 90° of amplitude. Regarding the damping, results of free decay tests performed for various amplitude showed that the structural damping behaves linearly in plunge but significantly increases in pitch for low angle of attack ($|\alpha| < 2$ deg), because of the solid friction induced by the bearings. As a consequence, the system can be affected by nonlinear behaviour of the setup at small amplitude in pitch. This will be discussed later.

Four different configurations have been studied (two section model and two position of the centre of rotation). The non-dimensional parameters of each configuration are reported in Tab. 1 with ω_h/ω_α the ratio of plunge to pitch natural frequencies, $r_G = \sqrt{I_\alpha/mb^2}$ the non-dimensional radius of gyration of the system about its elastic centre, $\mu = m/(\pi\rho b^2 E)$ the solid/fluid mass ratio (introducing *E*, the span of the model) and $x_\alpha = x_{CG}/b$ the non-dimensional distance from the elastic centre to the centre of gravity (counted positively

toward the trailing edge). Note that for each position of the centre of rotation mass and inertia have been adjusted to maintain the same value of x_α for both the flat-plate and NACA0018 configurations.

For each configuration the coupled-mode flutter critical reduced velocity $U_c^* = U_c/b\,\omega_\alpha$ has been calculated solving the eigenvalue problem of the aeroelastic system using the full linear Theodorsen's formulations[1)] for the motion induced lift and moment (see Bisplinghoff and Ashley[4)] and Amandolese et al[24)] for more details on the procedure). Results are reported on Table 1 along with the critical reduced velocity U_{TD}^* associated to torsional divergence static stability. According to those results each configuration should start to flutter for $U_c^* < 16$ and their post-critical behaviour can be studied up to 2.5 times the flutter critical velocity.

Table 1: Non-dimensional parameters of the four aeroelastic configurations

	ω_h/ω_α	r_G	μ	η_h	η_α	x_α	U_c^*	U_{TD}^*
FP1/4	0.805	0.695	2887	0.0008	0.01	0.12	15.2	/
FP1/2	0.792	0.684	2896	0.0008	0.01	0.06	13.8	36.8
N1/4	0.808	0.610	1996	0.0008	0.01	0.12	11.9	/
N1/2	0.785	0.593	2247	0.0008	0.01	0.06	11	28.1

3. LOW SPEED FLUTTER RESULTS

Experiments were performed in the velocity range of the wind tunnel ranging from 4 up to 30m/s (i.e. $Re \sim 1 - 8\times10^4$). For each configuration (a section model for a specific position of the axis of rotation), the bifurcation diagrams were identified as following: for a fixed wind tunnel speed the stability of the system is checked to small initial perturbations. If the system is stable the procedure is repeated for a higher velocity until the critical reduced velocity, U_c^*, is found. The dynamical response is then measured increasing the velocity up to a limit value and decreasing the velocity down to a lower critical velocity, U_c^{**}, for which the system is damped.

For each velocity beyond U_c^{**} the system reaches LCO regime for which frequency and amplitude in pitch and plunge have been measured. In some case the amplitude of the LCO are modulated with time. An « error bar » is then associated to each point reported on Figs 2-8 in order to appreciate the maximum value (top of the bar) and minimum value (bottom of the bar) of the LCOs amplitude.

(3.1) Flat-plate and NACA0018 section models for the elastic axis at the first quarter chord

The bifurcation diagrams, i.e. LCO amplitude in pitch and plunge versus the reduced velocity, are reported in Figs. 2 for the "FP14" configuration and Fig 3 for the "N14" configuration. For both configurations the elastic axis is set to the first quarter chord and apart from the mass ratio the non-dimensional aeroelastic parameters are close. Nevertheless one can clearly notice that the post-critical behaviours are strongly different.

For the flat-plate model with velocity increasing the system undergoes a first bifurcation for a critical velocity $U_c^* \approx 18$ which is 20% higher than the value predicted by the linear stability analysis. Following an initial small perturbation the system reaches a stable limit cycle oscillation regime of small amplitude in pitch, $\alpha_{LCO} \approx 5°$ and moderate amplitude in plunge $h_{LCO}/b \approx 0.13$ that increase almost linearly to reach values up to $\alpha_{LCO} \approx 10°$ in pitch and $h_{LCO}/b \approx 0.25$ in plunge at $U^* \approx 30$. Decreasing the reduced velocity the system remains in the same LCO branch down to a smaller critical velocity $U_c^{**} \approx 13$ for which the system is damped. This hysteretic behavior, suggesting a subcritical instability is certainly due to the structural nonlinearity induced by the bearings at low amplitude of rotation.

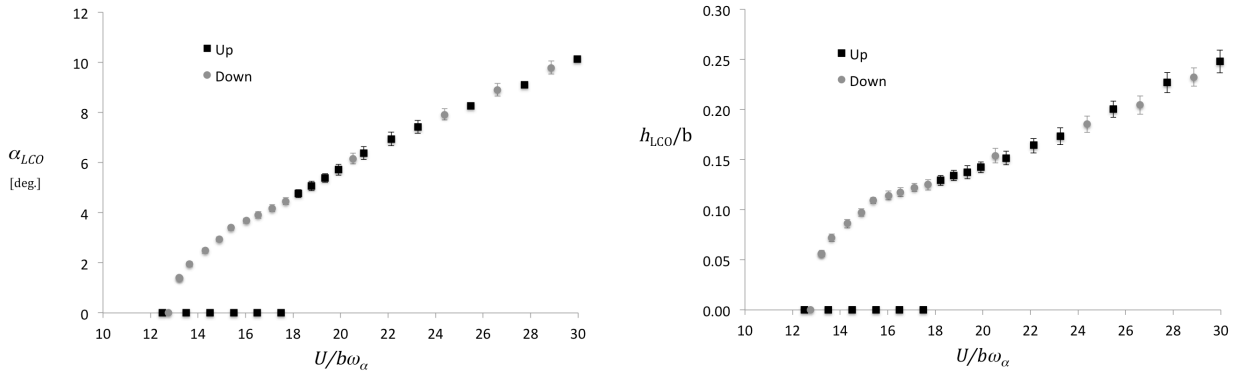

Figure 2: LCO amplitude in pitch (left) and plunge (right) versus the reduced velocity for the « FP14 » configuration: flat-plate section model with the elastic axis at the first quarter chord;.

For the NACA0018 model the dynamic of the system is strongly different. The system undergoes a first bifurcation for a critical velocity $U_c^* \approx 11$ which is 7.5% lower than the one predicted by the linear stability analysis. The system then follow a first LCO branch characterized by small amplitude of oscillation in pitch $3° < \alpha_{LCO} < 8°$ and moderate amplitude in plunge $0.09 < h_{LCO}/b < 0.12$. For a reduced velocity $U^* \approx 16$ the system undergoes a second bifurcation and switches to a LCO branch characterized by higher amplitude in pitch $30° < \alpha_{LCO} < 35°$ and amplitude in plunge that gradually increases with the reduced velocity up to $h_{LCO}/b \approx 0.19$ at $U^* \approx 25$. Decreasing the reduced velocity the system remains in the second LCO branch down to a critical velocity $U_c^{**} \approx 11.3$ for which it goes back to the first LCO branch.

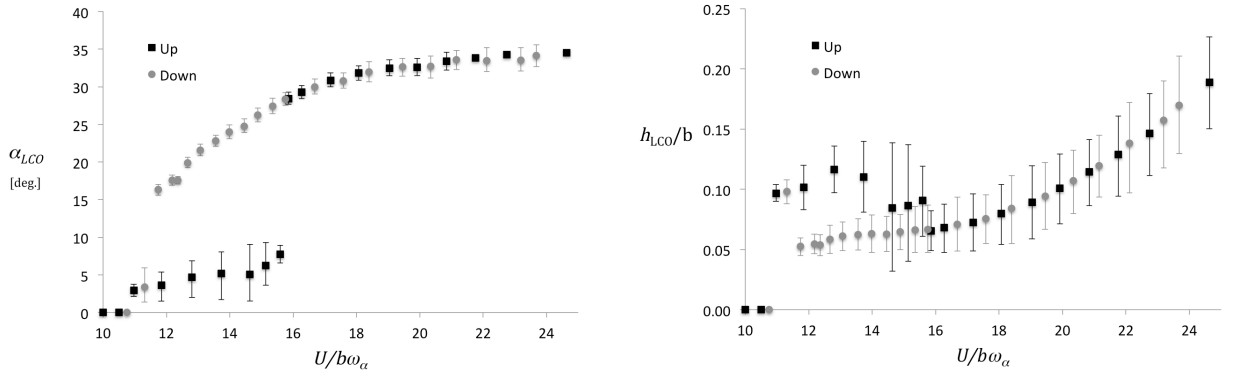

Figure 3: LCO amplitude in pitch (left) and plunge (right) versus the reduced velocity for the « N14 » configuration: NACA0018 model with the elastic axis at the first quarter chord.

LCOs frequencies evolution with the reduced velocity are reported in Fig. 4 for both the « FP14 » and « N14 » configurations. It is iterresting to notice that for the flat-plate model the couple mode flutter frequency start close to the plunge natural frequency and gradually increases with the reduced velocity. Those results are in accordance with the linear statbility ananlysis that predicts a destabilization of the plunging branch of the system. On the other hand if the frequency evolution behaves the same way in the first LCO branch for the NACA0018 model, the switch to the second LCO branch is associated to a sudden increase of the frequency of oscillations that is now sligly over the natural frequency in pitch. Those results suggest that the second LCO branch is dominated by a symmetric stall flutter regime.

To further investigate the observed discrepancy between the flat plate and NACA0018 model the aeroelastic response of the NACA0018 profile have been tested in a one degree of freedom “pure pitch” configuration. The LCO amplitude evolution versus the reduced velocity is reported in Fig. 5. It clearly shows that the model experiences self-sustained oscillations of small amplitude in the reduced velocity range $9.5 < U^* < 16$. That kind of velocity bounded instability in pure pitch was first reported by Poirel[27,28] on a

NACA0012 section model at moderate Reynolds number $Re{\sim}4.5-13{\times}10^4$. According to Poirel it can be attributed to the motion-induced dynamics of a laminar separation bubble. In the light of these results it is then possible that the "N14" pitch-plunge configuration was significantly affected by a laminar separation flutter[28] process that can trig the first onset of flutter and plays a role in the quick entrance in the symmetric stall flutter regime.

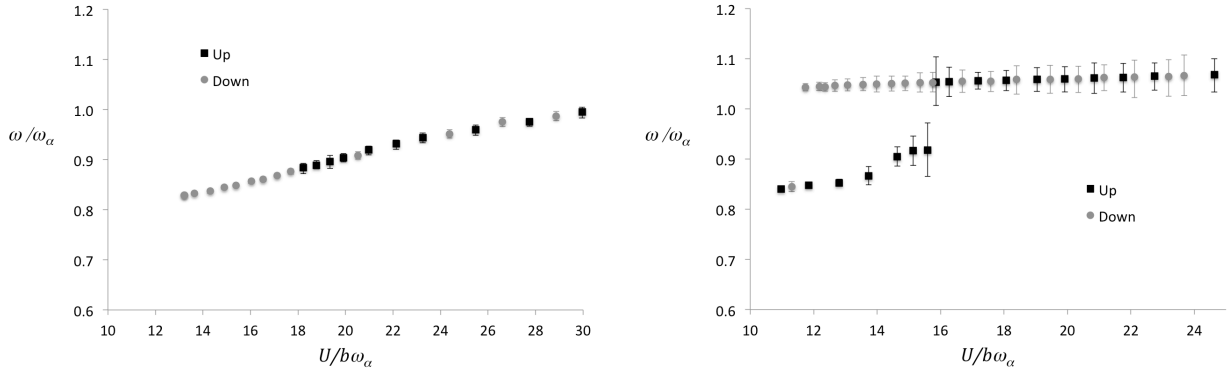

Figure 4: LCO frequency evolution versus the reduced velocity for the « F14 » configuration (left) and « N14 » configuration (right).

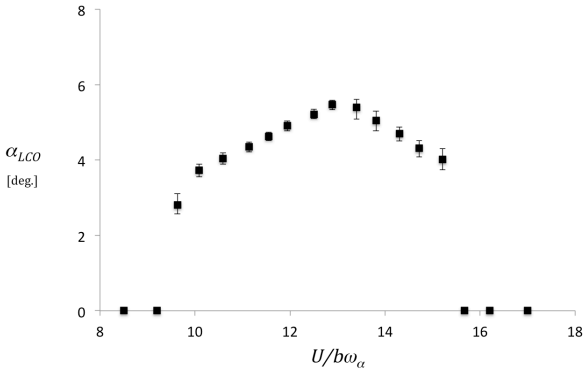

Figure 5: LCO amplitude versus the reduced velocity for the NACA0018 section model in pure pitch with the elastic axis at the first quarter chord.

(3.2) Flat-plate and NACA0018 section models for the elastic axis at the mid-chord

The bifurcation diagrams in pitch and plunge are reported in Figs. 6 for the "FP12" configuration and Fig 7 for the "N12" configuration. The elastic axis is set here at the mid-chord and as for the previous configurations, mass and inertia have been adjusted in order to set the main non-dimensional aeroelastic parameters as close as possible. Here again the flat-plate and NACA0018 models exhibit strongly different behaviours.

With the flat-plate model the system undergoes a first bifurcation for a critical velocity $U_c^* \approx 11.9$ which is 14% lower than the value predicted by the linear stability analysis. Increasing the wind velocity the system then follows a first stable LCO branch characterized by small and gradually increasing amplitude in pitch $2° < \alpha_{LCO} < 7°$ for $12 < U^* < 16$, and moderate amplitude in plunge that first increases to reach a top value $h_{LCO}/b \approx 0.22$ at $U^* \approx 14$. Beyond that reduced velocity the amplitude of oscillation in plunge decreases and is strongly modulated. The amplitude of modulation growths until $U^* \approx 16$ where the system switch to a second LCO branch characterized by high oscillations in pitch with amplitude that increases linearly up to $\alpha_{LCO} \approx 60°$ at $U^* \approx 20$. In the same time the amplitude of oscillation in plunge also increases with the reduced velocity but remain significantly modulated. Decreasing the reduced velocity from $U^* \approx 20$ the system remains in the second LCO branch down to almost the same critical velocity $U_c^{**} \approx 12$ for which the system is damped.

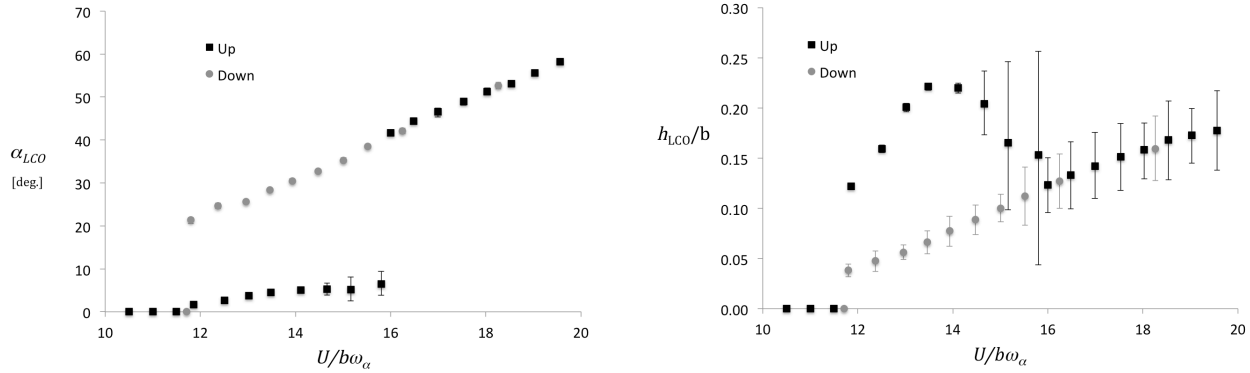

Figure 6: LCO amplitude in pitch (left) and plunge (right) versus the reduced velocity for the « FP12 » configuration: flat-plate section model with the elastic axis at the mid-chord.

For the NACA0018 model the dynamics of the system is strongly different. The system undergoes a first bifurcation for a critical velocity $U_c^* \approx 8$ which is 25% lower than the value predicted by the linear stability analysis. Beyond that critical point the system gradually follow a stable LCO branch characterized by moderate amplitude of oscillation in plunge but large amplitude of oscillation in pitch. At $U^* \approx 15$ the system reaches $\alpha_{LCO} \approx 65°$. The self-sustained response of the system in pure pitch configuration is also reported in Figure 7 (left). It clearly shows that the dynamic of the system is dominated by a pure pitch instability. The onset of this instability is certainly due to a laminar separation bubble fluttering process that trigs the system to a very energetic symmetric stall flutter regime.

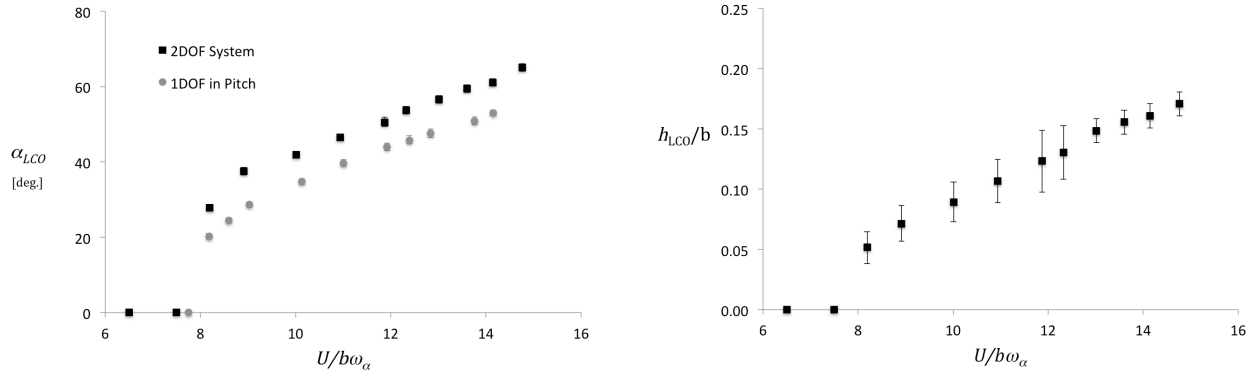

Figure 7: LCO amplitude in pitch (left) and plunge (right) versus the reduced velocity for the « N12 » configuration : NACA0018 section model with the elastic axis at the mid-chord.

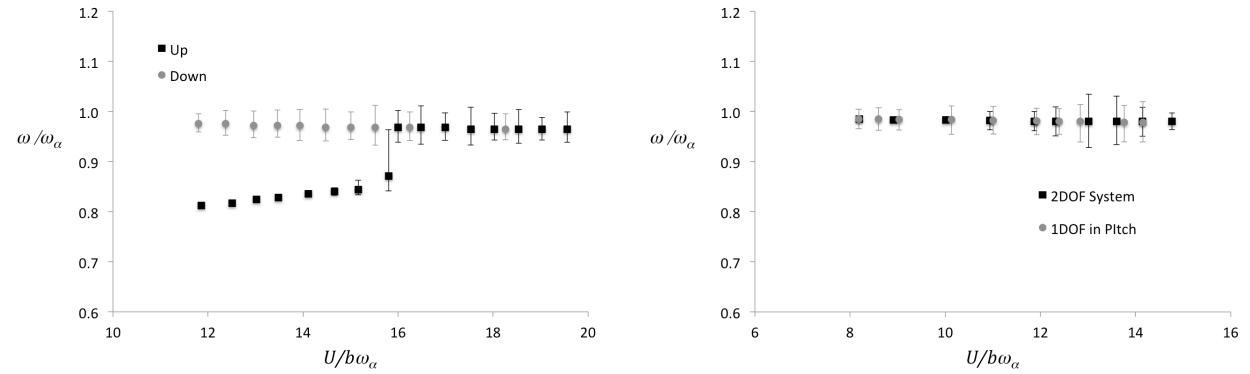

Figure 8: LCO frequency evolution versus the reduced velocity for the « F12 » configuration (left) and « N12 » configuration (right).

LCOs frequencies evolution with the reduced velocity are reported in Fig. 8 for both the « FP12 » and « N12 » configurations. For the flat-plate two frequency regimes are clearly highlighted: the first one is associated to the first coupled-mode flutter branch and the second one shows that the system is dominated by the natural ferquency in pitch and thus a stall flutter regime. For the NACA0018 configuration the system is fully dominated by a pure pitch istability and the LCO frequencies remains close to the natural frequency in picth.

4. CONCLUSIONS

The post-critical behaviour of two degree-of-freedom airfoils undergoing low speed flutter have been studied in wind tunnel for moderate Reynolds number $Re \sim 1 - 8 \times 10^4$. Tests have been performed on both flat-plate and NACA0018 section models, using an aeroelastic set-up that enables high amplitude pitch-plunge motion. For each section model two aeroelastic configurations have been studied : first for a centre of rotation at the first quarter chord and a non-dimensional distance from the elastic centre to the centre of gravity $x_\alpha \approx 0.12$ and second, for a centre of rotation at the mid-chord and $x_\alpha \approx 0.06$. Each configuration was designed to observe the onset of coupled-mode flutter at moderate reduced velocity $U_c^* < 16$ away from an eventual static divergence instability so that their post-critical behaviour can studied over a large velocity range. Results have been reported in term of bifurcation diagrams, i.e. LCOs amplitude and frequency evolution in both pitch an plunge versus the reduced velocity, increasing the velocity up to a limit value and then decreasing the reduced velocity down to stable position.

Results have highlighted strong discrepancies between the flat-plate and the NACA0018 section model. For both the elastic axis position, the flat-plate model first undergoes a coupled mode flutter in accordance with the prediction of linear stability analysis, i.e. a destabilisation of the heaving branch. For the elastic centre at the first quarter chord the system remains in a unique LCOs branch characterized by a low increasing amplitude in pitch and moderate amplitude in plunge up to a reduced velocity 2.5 time higher than the critical flutter velocity. For the elastic centre at the mid-chord the system switches to a symmetric stall flutter regime for $U^* \approx 1.4 \times U_c^*$ which is characterized by high amplitude in pitch and moderate amplitude in plunge that increase linearly with the reduced velocity.

For the NACA0018 model two LCOs branches have also been observed but here only for the configuration with the elastic axis at the first quarter chord. Indeed the dynamics of the system seems to be significantly enhanced by a laminar separation bubble fluttering process. For the configuration with the elastic axis at the mid-chord the post-critical flutter behaviour is then fully dominated by a pure pitch instability. The onset of this instability is certainly due to a laminar separation flutter that trigs the system to a strong symmetric stall flutter regime characterized by very high and stable limit cycle oscillations in pitch and moderate amplitude of oscillations in plunge.

ACKNOWLEDGMENT

The author gratefully acknowledges the DGA for its financial support through the DYSACCI project.

REFERENCES

1) Theodorsen, T. : General Theory of aerodynamic instability and the mechanism of flutter, *NACA Technical Report* 496, 1935.
2) Sears, W. R. : Some aspects of non-stationary airfoil theory and its practical application, *Journal of the Aeronautical Sciences,* Vol. 8, pp. 104-108, 1941.
3) Fung, Y.C. : An introduction to the theory of aeroelasticity, John Wiley and Sons, Inc., New-York, N.Y., 1955. Also available in Dover Edition.
4) Bisplinghoff, R. L., Ashley, H. : Principles of aeroelasticity, John Wiley and Sons, Inc., New-York, N.Y., 1962. Also available in Dover Edition.
5) Dowell, E.H., Clark, R., Cox, D., Curtiss, H.C., Edwards, J.W., Peters, D.A., Scanlan, R., Simiu, E., Sisto, F., Hall, K.C. and others : A modern course in aeroelasticity. Ed. Kluwer, U.S.A., 2004.

6) Naudascher, E. Rockwell, D. : Flow-induced vibrations: An engineering guide, Ed. Balkema, Netherlands, 1994.
7) Leishman, J. G. : Principles of Helicopter Aerodynamics, Cambridge university press, 2006.
8) Hansen, M.O.L., Sørensen, J.N., Voutsinas, S., Sørensen, N., Madsen, H.Aa. : State of the art in wind turbine aerodynamics and aeroelasticity, *Progress in Aerospace Sciences*, Vol. 42, Pt. 4, pp. 285-330, 2006.
9) McCroskey, W. J. : Unsteady airfoils. *Annual Review of Fluid Mechanics,* Vol. 14, pp. 285–311, 1982.
10) Li, J., Dimitriadis, G. : Experimental Study of Stall Induced LCOS of Free-Vibrating Wings, in *Proceedings of the CEAS International Forum on Aeroelasticity and Structural Dynamics*, Paper IF-026, Stockholm, 2007.
11) McCroskey, W.J., Philippe, J.J. : Unsteady viscous flow on oscillating airfoils, *AIAA Journal,* Vol. 13, Pt. 1, pp. 71–79, 1975.
12) Carr, L.W., McAlister, K.W., McCroskey, W.J. : Analysis of the development of dynamic stall based on oscillating airfoil experiments. *NASA-TN-D-8382*, 1977.
13) Dowell, E., Edwards, J., Strganac, T.W. : Nonlinear Aeroelasticity, *AIAA Journal of Aircraft*, Vol. 40, Pt. 5, pp. 857-874, 2003
14) Lee, B.H.K., Price, S.J., Wong, Y.S. : Nonlinear aeroelastic analysis of airfoils: bifurcations and chaos, *Progress in Aerospace Sciences*, Vol. 35, pp. 205-334, 1999.
15) Lee B.H.K., LeBlanc P. : Flutter analysis of a two-dimensional airfoil with cubic nonlinear restoring force. Aeronautical Note NAE-AN-36, NRC No. 25438, National Research Council of Canada, 1986.
16) Conner, M.D., Tang, D.M., Dowell, E.H., Virgin, L.N. : Nonlinear behavior of a typical airfoil section with control surface freeplay, *Journal of Fluids and Structures*, Vol. 11, Pt. 1, pp. 89-109, 1997
17) Schewe, G., Mai, H., Dietz, G. : Nonlinear effects in transonic flutter with emphasis on manifestations of limit cycle oscillations, *Journal of Fluids and Structures,* Vol. 18, pp. 3–22, 2003.
18) Ericsson, L.E., Reding, J.P. : Unsteady Airfoil Stall and Stall Flutter, NASA, CR 111906, 1971.
19) Dunn, P., Dugundji, J. : Nonlinear stall flutter and divergence analysis of cantilevered graphite/epoxy wings. *AIAA journal,* Vol. 30, Pt. 1, pp. 153-162, 1992.
20) Sarkar, S., Bijl, H. : Nonlinear aeroelastic behavior of an oscillating airfoil during stall induced vibration, *Journal of Fluids and Structures,* Vol. 24, pp. 757-777, 2008.
21) Dimitriadis, G., & Li, J. : Bifurcation behavior of airfoil undergoing stall flutter oscillations in low-speed wind tunnel, *AIAA journal*, Vol. 47, Pt. 11, pp. 2577-2596, 2009.
22) Razak, N. A., Andrianne, T., & Dimitriadis, G. : Flutter and stall flutter of a rectangular wing in a wind tunnel, *AIAA journal*, Vol. 49, Pt. 10, pp. 2258-2271, 2011.
23) Price, S.J., Fragiskatos, G. : Nonlinear aeroelastic response of a two-degree-of-freedom airfoil oscillating in dynamic stall, in: Ziada, S., Staubli, T. (Eds.), *Proceedings of the Seventh International Conference on Flow Induced Vibration*, Rotterdam, The Netherlands, pp. 437–444, 2000.
24) Amandolese, X., Michelin, S., & Choquel, M. : Low speed flutter and limit cycle oscillations of a two-degree-of-freedom flat plate in a wind tunnel, *J. Fluids and Structures*, Vol. 43, pp. 244-255, 2013.
25) Peng, Z., Zhu, Q. : Energy harvesting through flow-induced oscillations of a foil, *Physics of Fluids,* Vol. 21, 123602, 2009.
26) Bryant, M., & Garcia, E. : Modeling and testing of a novel aeroelastic flutter energy harvester, *Journal of vibration and acoustics*, Vol. 133, Pt. 1, 011010, 2011.
27) Poirel, D., Harris, Y., & Benaissa, A. : Self-sustained aeroelastic oscillations of a NACA0012 airfoil at low-to-moderate Reynolds numbers, *Journal of Fluids and Structures*, Vol. 24, Pt. 5, pp. 700-719, 2008.
28) Poirel, D., & Yuan, W. : Aerodynamics of laminar separation flutter at a transitional Reynolds number, *Journal of Fluids and Structures*, Vol. 26, Pt. 7, pp. 1174-1194, 2010.